Structure and Properties of Homogeneous Copolymers of Propylene and 1-Hexene

B. Poon,[†] M. Rogunova,[‡] A. Hiltner,* and E. Baer

Department of Macromolecular Science and Center for Applied Polymer Research, Case Western Reserve University, Cleveland, Ohio 44106-7202

S. P. Chum

Plastics R & D, The Dow Chemical Company, Freeport, Texas 77541

A. Galeski and E. Piorkowska

Centre of Molecular and Macromolecular Studies, Polish Academy of Sciences, Sienkiewicza 112, 90 363 Lodz, Poland

Received June 16, 2004; Revised Manuscript Received November 13, 2004

ABSTRACT: The solid state structure and properties of homogeneous copolymers of propylene and 1-hexene were studied by examining melting behavior, dynamic mechanical response, and morphology primarily with atomic force microscopy, wide- (WAXS) and small-angle X-ray scattering, and tensile deformation. Chain microstructure was analyzed by ^{13}C NMR. The results indicate that copolymers used in this study have an essentially random distribution of comonomer. For copolymers with less than 10 mol% hexane, crystallinity decreases with increasing comonomer content, as expected for exclusion of comonomer from the polypropylene crystal. The peak melting and crystallization temperatures also decrease with increasing hexene content. Copolymers with more than 10 mol% hexane crystallize with a new crystal structure that permits incorporation of hexene units. This is inferred from a higher level of crystallinity than would be expected if comonomer were excluded from the crystal and better development of the crystals as the hexene content increases. Copolymers with the new crystal structure crystallize slowly. After an incubation period, long fibrous lamellae form sheaf-like arrays that develop into small spherulites. The corresponding enthalpy change as a function of time assumes an S-shape characteristic of a phase transition described by the Avrami process. The new crystallographic form has not been reported for either polypropylene or for poly(1-hexene). It follows from WAXS studies of highly oriented films that the crystallographic unit cell has orthorhombic symmetry with $a = 1.9860$ nm, $b = 1.7176$ nm, and $c = 0.6458$ nm. The most intense diffracting planes are identified as the (210) plane reflecting at $2\theta = 10.30°$, the (230) plane reflecting at $2\theta = 17.65°$, the (040) plane reflecting at $2\theta = 20.60°$, the (031) plane reflecting at $2\theta = 20.73°$, and the (112) plane reflecting at $2\theta = 28.52°$ for Cu Kα radiation. On the basis of pole figures, it is evident that the easiest slip during plastic deformation of the new crystal form occurs along (0*k*0) planes.

Introduction

Recent advances in metallocene catalyst technology make possible olefinic copolymers with homogeneous, random insertion of comonomer units. New families of ethylene copolymers were developed[1,2] due to focus of the new technology on copolymerization of ethylene with α-olefins. Varying comonomer content allows a broad property range to be achieved, from HDPE-like thermoplastic behavior to elastomeric behavior.

The major interest in metallocene polymerization of propylene has been the wide variety of chain microstructures that can be synthesized in pure form, including hybrids of isotactic, syndiotactic, and atactic structures and different patterns of chain irregularities. Metallocene-catalyzed copolymerization of propylene has focused on copolymers with ethylene and dienes for the preparation of EP-type and EPDM-type elastomers.[3] Less is known about copolymers with higher α-olefins. With conventional Ziegler−Natta catalysts, comonomer incorporation is not uniform;[4] thus, the lower-molecular-weight fractions contain a higher percentage of comonomer and exhibit considerable solubility in hydrocarbons. On the other hand, metallocene propylene copolymers are chemically more homogeneous,[5] and show low levels of solubles even at high comonomer incorporation.[6]

The advantage of using metallocene catalysts is that copolymers with large amounts of comonomer can be synthesized. If the comonomer content is high enough that the crystallizable sequences are not long enough to chain fold into lamellar crystals, ethylene copolymers crystallize as fringed micellar crystals.[7] It is of interest to determine whether propylene copolymers similarly form fringed micellar crystals if the crystallizable sequences are short. Recently, copolymers of propylene with up to 30 mol% 1-octene were investigated.[8] In that study, increasing comonomer content reduced the ability of the material to crystallize and affected the mechanical behavior, which changed from thermoplastic to elastoplastomeric to elastomeric.

Metallocene copolymers with homogeneous comonomer distribution and narrow molecular weight distribution are convenient model systems for fundamental studies of structure−property relationships in semicrystalline olefinic copolymers. The melting temperature of metallocene-catalyzed propylene homopolymer (mPP)

* Author to whom correspondence should be addressed. E-mail: pah6@case.edu.
[†] Present address: The Dow Chemical Company, Freeport, TX.
[‡] Present address: PolyOne, Avon Lake, OH.

10.1021/ma048813l CCC: $30.25
Published on Web 01/15/2005

Table 1. Copolymers of Propylene and 1-Hexene

sample	hexene content (mol%)	M_w (kg mol^{-1})	M_w/M_n
mPP	0.0	185	2.7
PH2.2	2.2	276	2.3
PH3.1	3.1	296	2.0
PH4.8	4.8	249	2.2
PH9.7	9.7	207	2.0
PH13.5	13.5	168	2.1
PH13.9	13.9	148	1.9
PH22.4	22.4	123	2.0
PH25.1	25.1	129	2.0

is usually lower than the melting temperature of polypropylene synthesized with Ziegler−Natta catalysts (znPP). It is generally understood that the molecular architecture of mPP differs somewhat from that of znPP by having a narrower molecular weight distribution and a more homogeneous distribution of tactic defects.[9,10] In contrast to mPP, nonuniform distribution of defects in znPP produces chains with long defect-free regions. Crystallization of such segments results in more-ordered crystals and thicker lamellae, giving znPP a higher melting temperature.[11] A recent paper by Shin et al.[12] describes the synthesis and characterization of copolymers of propylene and 1-hexene. Although the catalyst used in this study was thought to produce random copolymers, the propylene homopolymer showed a relatively high melting temperature, indicating that the homogeneity in defect distribution was not as high as is usually achieved for metallocene catalysts.

The present study focuses on copolymers of propylene and with up to 25 mol% 1-hexene. The copolymers investigated were synthesized using metallocene catalysts which, we believe, will produce copolymers with more homogeneous distribution of 1-hexene units than those described previously.[12] The combined observations of solid-state structure and properties are used to understand the behavior of these materials.

Experimental Section

Experimental polypropylene and copolymers of propylene with 1-hexene, synthesized by a single-site catalyst technology, were provided by The Dow Chemical Company, together with information on copolymer composition, molecular weight, and molecular weight distribution as given in Table 1. The homopolymer is designated as mPP, and the copolymers are designated as PH followed by the mole percent hexene.

Samples for ^{13}C NMR analysis were prepared by adding approximately 3 g of a 50:50 mixture of tetrachloroethane-d_2/orthodichlorobenzene to 0.4 g polymer in a 10 mm NMR tube. The samples were dissolved and homogenized by heating the tube and its contents to 150 °C. The data were collected using a Varian Unity Plus 400 MHz spectrometer, corresponding to a ^{13}C resonance frequency of 100.6 MHz. The data were acquired using 4000 transients per data file, a 6 s pulse repetition delay, spectral width of 24 200 Hz and a file size of 64K data points, with the probe head heated to 130 °C.

Films 0.4 mm thick were compression molded from pellets. The pellets were sandwiched between Mylar sheets and heated at 190 °C for 10 min under minimal pressure, for 10 min at 10 MPa, and cooled to ambient temperature at approximately 15 °C min^{-1} in the press. Aging associated with slow crystallization, especially noticeable in copolymers with higher hexene content, was followed by the gradual increase in yield stress. A constant value was achieved after about a week of storage at ambient temperature. Thus, all films were aged for 7−12 days before the physical properties were measured.

Specimens weighing 5−10 mg were cut from the compression-molded films for thermal analysis, which was performed on a Perkin-Elmer Model 7 DSC. Thermograms were obtained from −50 to 190 °C with a heating/cooling rate of 10 °C min^{-1}. The first heating thermogram, the cooling thermogram, and the second heating thermogram were recorded. Crystallinity based on polypropylene was calculated from the heat of melting using a value of 209 J g^{-1} for the heat of fusion of the polypropylene crystal (ΔH_m^o).[13] Alternatively, the melted specimen was quenched in the DSC to −50 °C, and the glass transition temperature was determined from the subsequent thermogram obtained at a heating rate of 10 °C min^{-1}. Quenched specimens were also allowed to age at ambient temperature for various periods of time before the thermogram was recorded in order to obtain the crystallization kinetics.

Dynamic mechanical thermal analysis was carried out with a Polymer Laboratories dynamic mechanical thermal analyzer. Specimens in the form of rectangular pieces with dimensions of 17 mm × 7 mm were cut from compression-molded film and tested in dynamic tension with 1% strain at 1 Hz from −80 to 10 °C below the melting point.

The stress−strain behavior in uniaxial tension was measured with ASTM D1708 microtensile specimens cut from the films. Specimens were stretched in an Instron at a rate of 100% min^{-1}. Engineering stress and strain were defined conventionally.

Specimens for light microscopy were made by sandwiching a pellet between two glass slides, heating at 190 °C for 5 min under minimal pressure, and slowly cooling to ambient temperature at 3 °C min^{-1} on the hot stage of the optical microscope. After 1 day at ambient temperature, polarized light microscopy was performed on the specimens with the Olympus BH-2 microscope. For birefringence measurements, a λ/4-plate was used. Positive birefringence occurred when the spherulite quadrants with the higher-order polarization color were parallel to high index direction of the λ/4-plate; negative birefringence occurred when they were perpendicular.[14]

Specimens with free surfaces for atomic force microscopy (AFM) were prepared by melting the copolymer on a glass slide and cooling slowly at a rate of 3 °C min^{-1}. The thickness of the polymer film was at least 10 times the spherulite diameter. Specimens were aged for 2−3 days at ambient temperature before they were examined in the AFM. Alternatively, PH25.1 was quenched from the melt, and the same area of the free surface was imaged periodically over time to characterize the morphology changes during aging at ambient temperature. The AFM experiments were conducted in air with a commercial scanning probe microscope Nanoscope IIIa (Digital Instruments, Santa Barbara, CA) operating in the tapping mode. Measurements were performed at ambient conditions using rectangular diving-board-type Si probes with a spring constant of 50 N m^{-1} and resonance frequencies in the 284−362 kHz range. The tip radius was 10 nm. Height and phase images were recorded simultaneously; the spherulite structure was more apparent in height images; lamellar morphology was better revealed by modulus differences in phase images.

The crystal structure of compression-molded films was studied using wide-angle X-ray diffraction (WAXS) and small-angle X-ray scattering (SAXS). A WAXS system consisted of a computer-controlled wide-angle goniometer coupled to a sealed-tube source of Cu Kα radiation operating at 30 kV and 30 mA (Philips). The Cu Kα line was filtered using electronic filtering and the usual thin Ni filter. The slit system that was used for collecting 2Θ scans allowed for collection of the diffracted beam with a divergence angle of less than 0.05°. The position of X-ray peaks was calibrated by measuring the X-ray peaks from a thin layer of aluminum powder deposited on the surface of each specimen.

The previewing measurements of the crystal orientation were performed using a WAXS pinhole camera coupled to the X-ray generator (sealed-tube, fine point Cu Kα), Ni-filtered source operating at 30 kV and 50 mA (Philips) with imaging plates for recording the diffraction patterns. The imaging plates were placed perpendicular to the incident X-ray beam at a distance of 50 mm from the specimen. Exposed imaging plates (Fuji) were read with a PhosphorImager SI system (Molecular Dynamics). Crystallographic form was determined

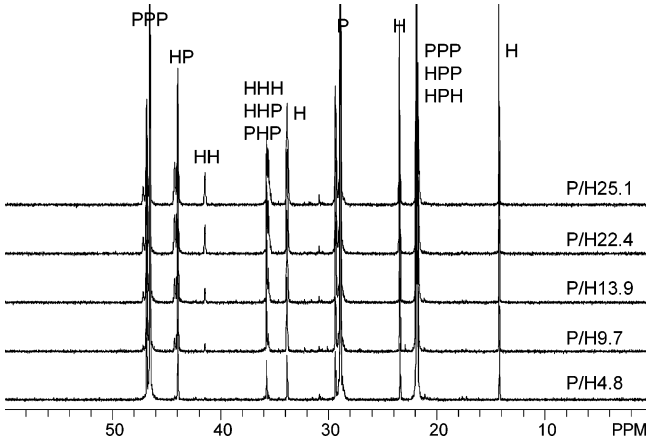

Figure 1. ^{13}C NMR spectra of selected PH copolymers.

on the basis of wide-angle diffraction patterns of oriented films.

Lamellar packing was probed by 2-D SAXS. The 1.1 m long Kiessig-type vacuum camera was equipped with a capillary collimator (X-ray Optical Systems, Inc.) and the imaging plate as a recording medium (Kodak). The camera was coupled to the X-ray generator (sealed-tube, fine point Cu Kα, Ni-filtered source operating at 50 kV and 40 mA) (Philips). The capillary collimator allowed for the resolution of scattering objects up to 40 nm. Exposed imaging plates were analyzed with a PhosphorImager SI system (Molecular Dynamics).

Orientation of crystalline phases in oriented films was studied by means of X-ray diffraction with pole figures. A WAXS system consisting of a computer-controlled pole figure device associated with a wide-angle goniometer coupled to a sealed-tube X-ray generator operating at 30 kV and 30 mA was used in this study. The X-ray beam consisted of Cu Kα radiation filtered by a Ni filter and electronically by setting threshold to proportional detector. The complete pole figures were obtained for the projections of Euler angles of sample orientation with respect to the incident beam, polar angle varying from 0° to 90° in 5° intervals and azimuthal angle varying from 0° to 360° in 5° steps. The construction of complete pole figures required the connection of the X-ray data collected in both transmission and reflection modes. The connection angle was polar angle equal to 50°, i.e., the reflection mode was used for polar angle from 0° to 50°, and the transmission mode for polar angle from 50° to 90°. The slit system of the diffractometer was adjusted to measure the integral intensity of the appropriate diffraction peak. The necessary corrections for background scattering and sample absorption were introduced. The diffraction data were further corrected for X-ray beam defocusing due to sample tilt and other instrumental effects using the data obtained at identical experimental conditions for random (unoriented) standard specimens. Details of the pole figure determination procedure were described elsewhere.[15] The pole figure plots were generated by the POD program, a part of the popLA package (Los Alamos National Laboratory, Los Alamos, NM). For every plot, the data were normalized to the random distribution density.

Results and Discussion

NMR Analysis. Selected ^{13}C NMR spectra are shown in Figure 1. The spectra corresponded with those reported previously for random copolymers of propylene and 1-hexene.[16,17] As expected for random substitution, the HH diad concentration increased smoothly with increasing hexane content as 0.00, 0.24, 0.60, 1.39, and 1.81 mol% for PH4.8, PH9.7, PH13.9, PH22.4, and PH25.1. Features of the poly(1-hexene) spectrum, which would have suggested a blocky microstructure, were absent.[18] Evaluation of the product of reactivity ratios, r_P and r_H, using the first-order Markovian model was close to unity, which further supported random distribution of comonomer.

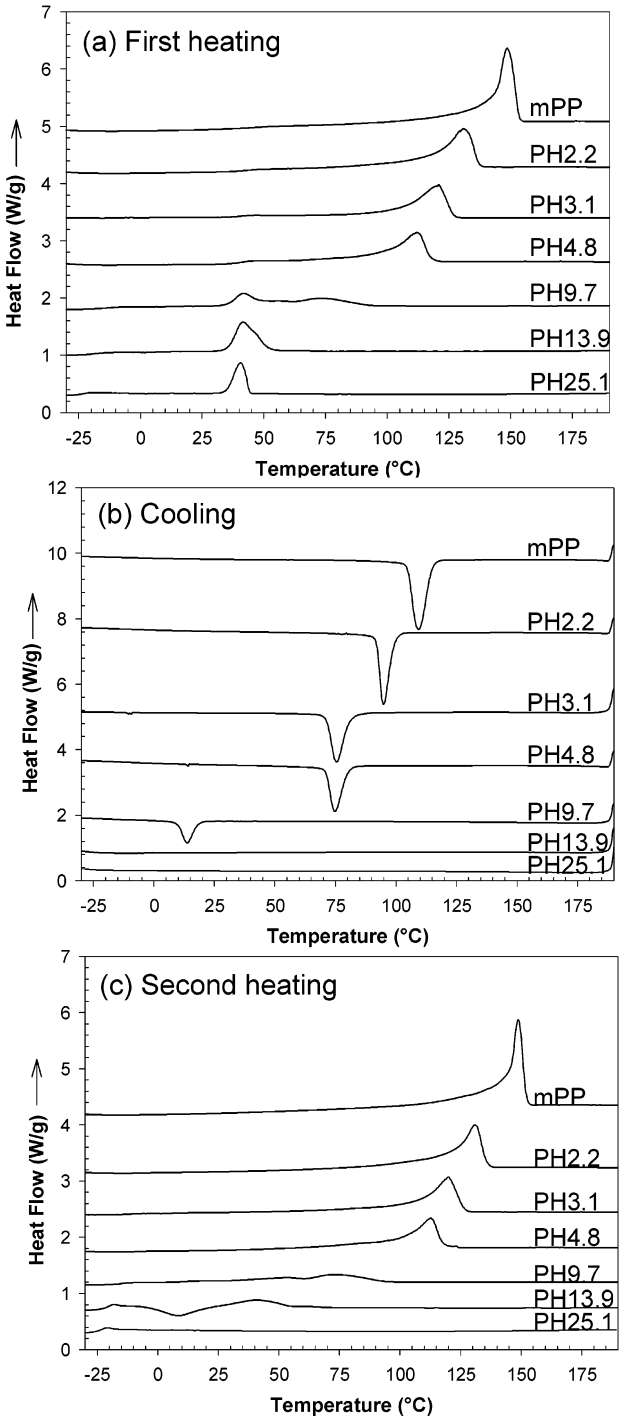

Figure 2. Thermal behavior of PH copolymers: (a) first heating thermograms; (b) cooling thermograms; and (c) second heating thermograms. Specimens were aged 7−12 days after compression molding. The heating/cooling rate was 10 °C min^{-1}.

Thermal Behavior. The first heating thermogram obtained after aging for 7−12 days, the cooling thermogram, and the second heating thermogram for mPP and PH copolymers are shown in Figure 2. The melting temperature of the metallocene-catalyzed homopolymer (mPP) of 149 °C was 10−15 °C lower than the melting temperature of polypropylene synthesized with Ziegler−Natta catalysts (znPP). This agrees with the general understanding that the molecular architecture of mPP,

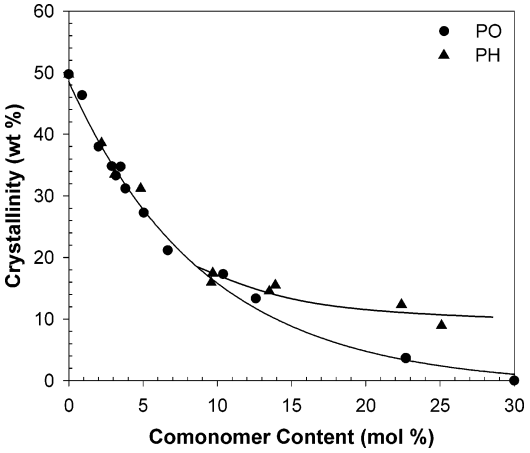

Figure 3. Crystallinity from DSC as a function of comonomer content for homogeneous PH and PO copolymers. Data for PO copolymers from ref 8.

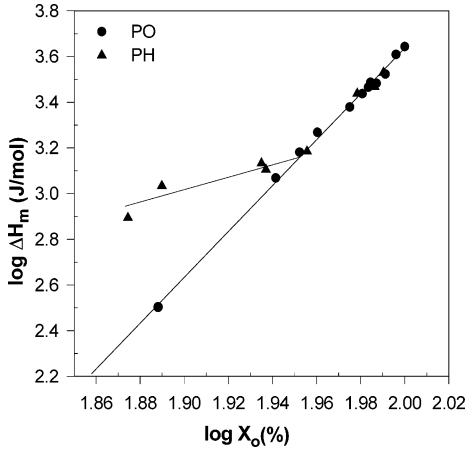

Figure 4. Logarithmic plot of the DSC heat of melting versus mole percent comonomer for PH and PO copolymers. Data for PO copolymers from ref 8. The solid line has slope of 10.

with narrower molecular weight distribution and more homogeneous distribution of tactic defects than znPP,[9,10] should lead to thinner lamellae, giving mPP a lower melting temperature.[11]

Incorporating up to 10 mol% hexene systematically decreased the melting temperature, broadened the melting range, and lowered the heat of melting during the first heating. Copolymers having 2.2, 3.1, and 4.8 mol% of hexene units had melting peaks at 131, 120, and 112 °C, respectively. The PH copolymers used in the present study had considerably lower melting temperatures than those of Shin et al.,[12] who reported a melting point of 136 °C for a copolymer with even higher hexene content of 7 mol%. Thus, comonomer had a larger effect on crystal size and perfection in the copolymers studied by us, pointing to a more homogeneous comonomer distribution. The first heating thermogram of PH9.7 had a very broad melting peak centered at about 75 °C and a second peak at about 40 °C. Copolymers with between 10 and 25 mol% hexene exhibited a relatively sharp melting peak at about 40 °C with relatively constant heat of melting, Figure 2a. All copolymers with less than 10 mol% hexene exhibited a crystallization exotherm in the cooling thermogram, although the crystallization temperature decreased with increasing comonomer content and, in the case of PH9.7, was lower than ambient temperature. In the case of copolymers with less than 5 mol% hexene, the undercooling was typically 40 °C, whereas crystallization of PH9.7 occurred at 15 °C, an undercooling of about 60 °C. A cooling rate of 10 °C min^{-1} was too rapid for copolymers with more than 10 mol% hexene to crystallize before reaching the glass transition temperature. In the subsequent heating curve, PH13.9 showed a cold-crystallization exotherm centered at 10 °C followed by melting. Crystallization of PH22.4 (not shown) and PH25.1 was too slow to occur during heating at 10 °C min^{-1}. Thus, the pronounced endothermic peak at about 40 °C on first heating thermograms of PH13.9 and PH25.1 was associated with melting of crystals formed during aging at ambient temperature.

Similar trends were observed in copolymers of propylene with 1-octene (PO), except that a copolymer with 22.7 mol% octene attained only about 4% crystallinity, and only after isothermal crystallization at −10 °C, and no crystallization was detected in a copolymer with 30 mol% octene. The relationship between comonomer content and crystallinity in Figure 3 compares PH copolymers with PO copolymers.[8] For this purpose, the crystallinity was determined from the heat of melting in the first heating thermogram. The crystallinity of PO copolymers decreased smoothly with comonomer content, as expected for a comonomer that is excluded from the crystal. The PH copolymers followed the same trend if the comonomer content was less than 10 mol%. However, PH copolymers with more than 10 mol% hexene exhibited higher levels of crystallinity than that anticipated for a comonomer that is completely excluded from the crystal lattice.

The relationship between comonomer content and heat of melting of olefinic copolymers often follows the relationship

$$\Delta H_m = k(X_o)^n \tag{1}$$

where X_o is mole percent of the crystallizing olefin, k is a constant related to the crystallinity of the olefin homopolymer, and n is sometimes interpreted as the minimum crystallizable sequence length.[19] A linear relationship was observed between log ΔH_m and log X_o for the PO copolymers, Figure 4. The extracted n value of 10 is consistent with the value of 11 found for polypropylenes of different tacticity.[20] Ethylene copolymers typically exhibit larger values of n.[21] For example, n values of 13 were observed for copolymers of ethylene with styrene (ES) and octene (EO).[1,2] Heat of melting of PH copolymers followed the same relationship with comonomer content as PO copolymers if the comonomer content was less than 10 mol%. Unexpectedly high crystallinity of copolymers with more than 10 mol% hexene content suggested that the assumption of comonomer exclusion did not hold at higher comonomer content. Crystallinity of the PH copolymers with more than 10 mol%, determined from the first heating thermogram, was associated with slow crystallization during aging at ambient temperature. The melting behavior suggested that if the hexene content was less than 10 mol%, comonomer was excluded from the crystal; however, if the comonomer content was higher, the crystallization habit changed so as to accommodate hexene units in the crystal lattice.

The dynamic mechanical relaxation behavior is presented as the temperature dependence of tan δ in Figure 5. For mPP, there were two relaxation peaks. The α-relaxation at approximately 80 °C represented a premelting phenomenon associated with increased mo-

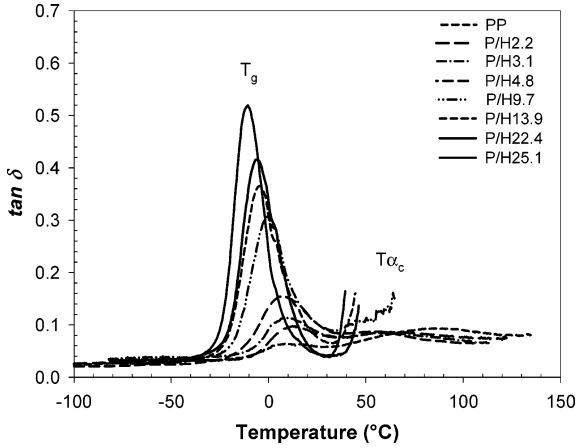

Figure 5. Dynamic mechanical relaxation behavior of PH copolymers presented as tan δ.

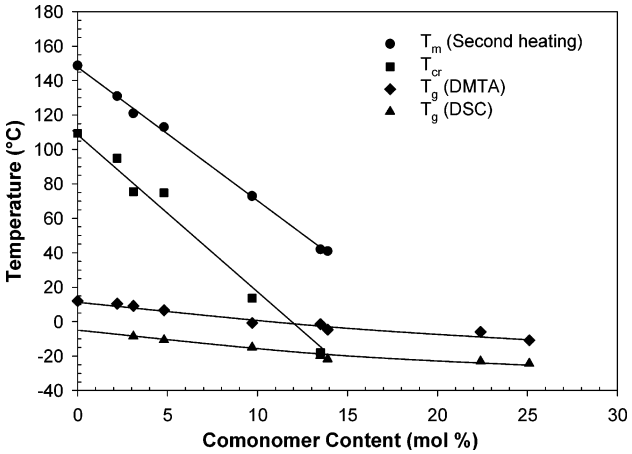

Figure 6. Effect of hexene content on melting temperature and glass transition temperature. The peak melting temperature, T_m, is taken from the second heating thermogram (Figure 2c). The crystallization temperature, T_{cr}, is taken from the cooling thermogram. The glass transition temperature, T_g, is taken from the peak in tan δ at 1 Hz (Figure 5) and from the DSC thermogram of the quenched specimens.

bility of chain segments in the crystal and in the interfacial region between the crystalline and amorphous phases.[22] The α-relaxation was also present, although at a slightly lower temperature, in copolymers with up to about 10 mol% hexene.

The β-relaxation at 12 °C corresponded to the glass transition of mPP. The low intensity of the peak resulted from the high crystallinity of mPP. With increasing hexene content, the peak increased in intensity and gradually shifted to lower temperatures, Figure 6. In the same Figure 6, the dependence of T_g on hexene content based on the DSC thermogram is plotted. Factors that contributed to the decrease in T_g were reduced crystalline constraint on the amorphous phase and the copolymer effect. Analysis of the copolymer effect by fitting T_g obtained from DSC to the Fox equation gave the T_g of polypropylene as −6.5 °C and T_g of poly(1-hexene) as −49.4 °C The same procedure applied to DMTA data gave +8.2 °C and −39.5 °C for polypropylene and poly(1-hexene), respectively. The T_g of polypropylene from fitting compared closely to reports of T_g for atactic polypropylene at −14 °C from heat capacity measurement,[23] and at −6 °C from DSC.[24] The T_g of amorphous poly(1-hexene) from DMTA measurements at 100 Hz is reported at −36.6 °C.[12]

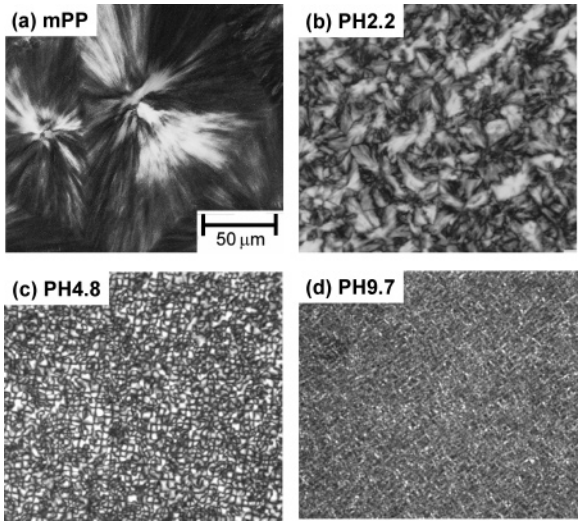

Figure 7. Polarized optical micrographs of PH copolymers: (a) mPP; (b) PH2.2; (c) PH4.8; and (d) PH9.7.

Peak melting temperature from the second heating thermogram and crystallization temperature T_{cr} from the cooling thermogram are included in Figure 6 with data for T_g. Steric hindrance was one factor that impeded crystallization as comonomer content increased. In addition, the crystallization temperature decreased more rapidly than the glass transition temperature. As the crystallization temperature approached the glass transition temperature, loss of segmental mobility further retarded crystallization.

Solid State Morphology. The mPP formed large spherulites with an average diameter of about 100 μm and a birefringence pattern in the polarizing light microscope that identified them as α-positive spherulites, Figure 7a. Positive birefringence identified the predominant chain direction as radial. With the chain direction perpendicular to the lamellar surface, most of the lamellae were oriented tangentially to the spherulite growth direction. As is typical for homogeneous copolymers, the spherulites became smaller with increasing hexene content, Figure 7b−d. The α-positive spherulites of PH2.2 were about 50 μm in diameter. The size of the spherulites was related to the crystallization temperature and undercooling. From the DSC data (Figure 6), the copolymers showed decreasing melting temperature and decreasing crystallization peak temperature with increasing hexene content, both related to retarding of segmental diffusion by hexene units. However, the lower crystallization temperature of the copolymers allowed for the formation of more nuclei in the copolymers.

Increasing the hexene content to 4.8 and 9.7 mol% decreased the spherulite size further, Figure 7c,d. It also changed the sign of birefringence from positive to negative, indicating that changes occurred to the internal spherulitic organization. In these copolymers, secondary crystallization by crystallographic branching from radial lamellae either did not occur or was too slow to be noticeable within the aging times used to prepare the specimens. Birefringence was detected in copolymers with higher hexene content of 13.9, 22.4, and 25.1 mol% (not shown); however, the structures were too small to be resolved in the polarizing light microscope.

Atomic force microscopy (AFM) height images of free surfaces in Figure 8a−e show the spherulitic size scale, and higher-resolution phase images show the lamellar size scale. Spherulites of mPP were approximately 100

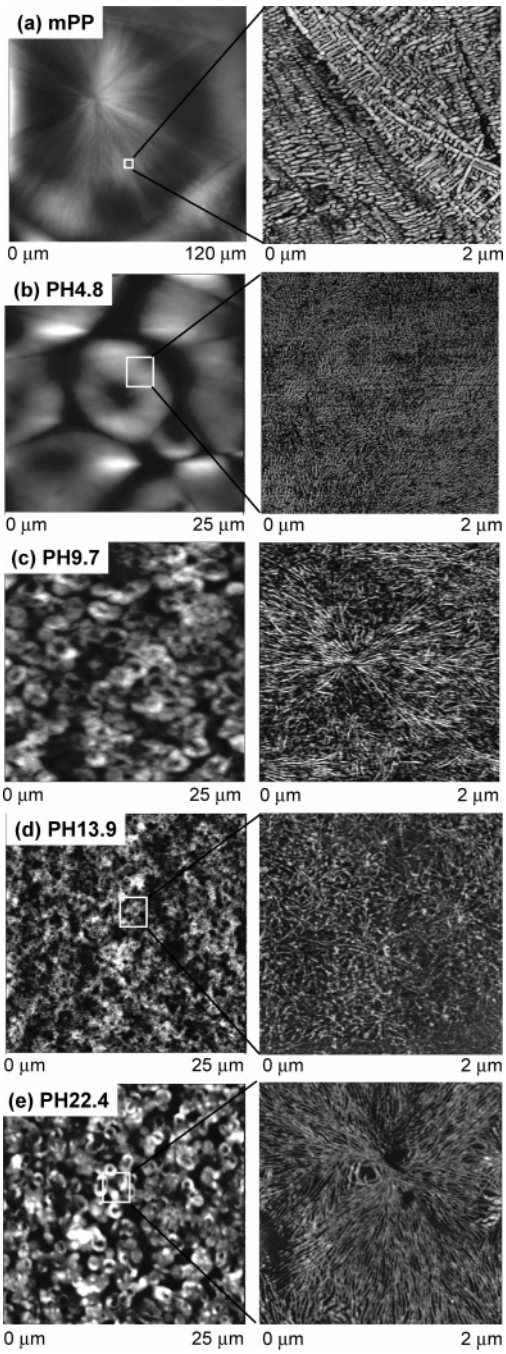

Figure 8. AFM height and phase images of free surfaces: (a) mPP; (b) PH4.8; (c) PH9.7; (d) PH13.9; and (e) PH22.4.

μm in diameter (Figure 8a), comparable to the OM observation (Figure 7a). Radial lamellae were very long and thick, in the range of 25−30 nm in thickness. Densely packed tangential lamellae confirmed the interpretation of the optical birefringence pattern. These lamellae formed by crystallographic branching from the (010) plane of radial lamellae.[25] They produced the characteristic lamellar texture commonly known as crosshatching.[26]

Spherulites of PH4.8 were impinging donut-shapes approximately 10 μm in diameter (Figure 8b). Similar donut-shaped spherulites of PH9.7 (Figure 8c) were smaller, about 2 μm in diameter, and were almost completely space-filling. The centers of spherulites were lower than the surrounding material which was pulled out of the melt during crystallization. This caused the

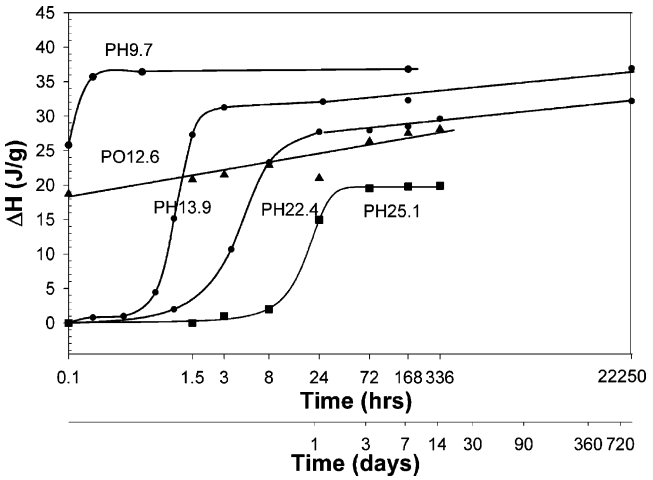

Figure 9. Effect of ambient temperature aging on heat of melting of PH copolymers with high hexene content. Data for a PO copolymer with 12.6 mol% octene is plotted for comparison.

depression between spherulites, enhanced by volume shrinkage during crystallization at the free surface. Lamellae of PH4.8 and PH9.7 were oriented radially, which confirmed the interpretation of the negative optical birefringence. The lamellae were short and thin, about 14 nm thick for PH4.8 and 11 nm thick for PH9.7. Morphological observations of PH copolymers in this copolymer composition range closely mimicked the spherulitic and lamellar characteristics of PO copolymers described previously.[8]

The low-resolution image of PH13.9 contained some small nascent spherulites about 2 μm in diameter (Figure 8d). A higher-resolution image revealed some long lamellae in an overall texture of short branched lamellae. Surprisingly, the low-resolution image of PH22.4 (Figure 8e) showed donut-shaped spherulites that were only slightly smaller than the spherulites of PH9.7 and were better formed than the nascent spherulites of PH13.9. A higher-resolution image of one spherulite revealed long, well-organized lamellae extending radially from the center. The lamellae were 10−15 nm thick, slightly thicker than lamellae of PH9.7.

Crystallization Kinetics. Propylene copolymers typically exhibited a certain amount of aging at ambient temperature, which included a small increase of secondary crystallization. Accordingly, molded specimens were aged for a period of time, 7−12 days in this study, before making measurements. The effect of ambient temperature aging on crystallization of PH with comonomer content near or above 10 mol% is presented in Figure 9. The heat of melting was determined from the single melting peak at 35−40 °C for PH copolymers with more than 10 mol% hexene and from the two peaks at 40−45 °C and 75−80 °C for PH9.7. Isothermal crystallization at ambient temperature revealed an induction period on the time-scale of few hours followed by a period of rapid crystallization during which close to the maximum crystallinity was achieved in a relatively short period of time. The enthalpy change as a function of time assumed the S-shape characteristic for the phase transition described by the Avrami process, i.e., consisting of nucleation and growth.

The induction period lengthened with increasing hexene content. It is seen that PH9.7 crystallized at ambient temperature in a few minutes, PH13.9 in 3 h, and PH22.4 in 10−12 h, whereas PH25.1 required a full

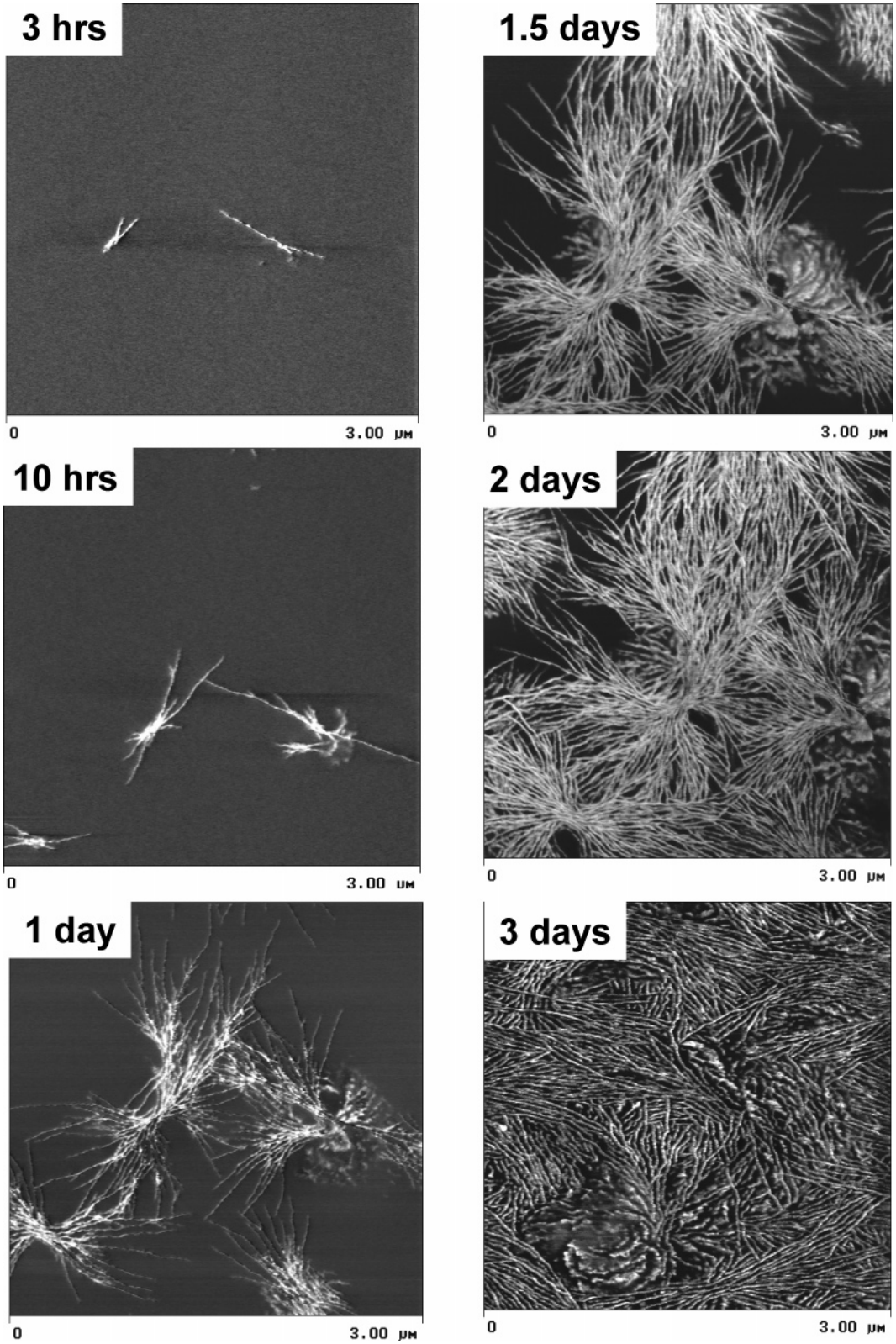

Figure 10. AFM phase images of the same location on a PH25.1 free surface after aging at ambient temperature for various periods of time.

day. Slow crystallization of PH13.9 and PH22.4 continued even after 2.5 years. A comparison with propylene–octene copolymers of similar comonomer content showed that PH13.9 crystallized more slowly than PO12.6. Indeed, PO12.6 crystallized during quenching to ambient temperature and the results included in Figure 9 show the typical logarithmic increase in secondary crystallinity with time.[8] However, PO22.7 had only a trace of crystallinity and PO30.0 did not crystallize, whereas PH22.4 and PH25.1 crystallized readily on the laboratory time scale.

The series of AFM images in Figure 10 shows the same region of a PH25.1 specimen at different time intervals as it aged at ambient temperature. After 3 h, lamellar crystallization had nucleated at two positions; after 10 h, the lamellae had grown in length and

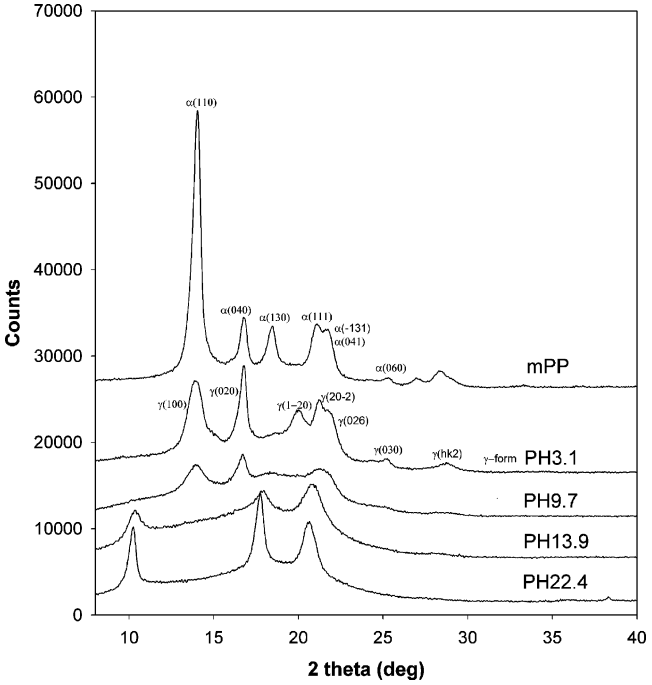

Figure 11. WAXS diffractograms collected in reflection for PH films. The reflections of the α and γ crystallographic forms of isotactic polypropylene are identified.

additional lamellae were growing from the same site. A new nucleation site at the lower left corner appeared which was not present in the 3 h image. After 1 day, the lamellae were longer, branched, and more numerous, and the lamellar aggregates had taken on a sheaf-like organization. With time, the sheafs expanded primarily from the initial nucleation sites until they were space-filling at 3 days. The long, thin, well-defined lamellae of PH13.9 contrasted sharply with the random dispersion of lamellar-like structures in an overall granular texture that characterized the crystalline morphology of PO12.6.[8] Differences in crystallinity, crystallization kinetics, and crystalline morphology suggested that PH copolymers with more than 10% comonomer were unusual.

Crystal Structure. The 2θ scans in reflection for compression-molded films are collected in Figure 11. For mPP, the peaks from the monoclinic α-form iPP crystals are clearly recognizable. A faint trace of the peak typical of hexagonal β-form iPP crystals at $2\theta = 16°$ is visible on the shoulder of the α-form peak for the (040) plane. There was no change in the diffraction pattern for mPP after aging for 24 h or longer at ambient temperature after compression molding.

For the PH3.1 film, the diffraction pattern changed dramatically compared to the pattern for mPP. The (130) peak almost disappeared, whereas a new peak at $2\theta = 20.07°$ emerged. These two alterations indicated formation of the γ-phase of iPP. It appeared that the PH3.1 film contained almost exclusively γ crystals. The diffracting planes of the α and γ crystallographic forms of iPP are identified in Figure 11 (monoclinic α-form with $a = 0.665$ nm, $b = 2.096$ nm, $c = 0.650$ nm, and $\beta = 99.3°$;[27] orthorhombic γ-form with $a = 0.854$ nm, $b = 0.993$ nm, and $c = 4.241$ nm,[28−30]).

The γ-form almost disappeared from the PH9.7 film, as seen from the absence of the (117) reflection at $2\theta = 20.07°$. The existing crystals were identified as a highly defective α crystallographic form. The degree of crystallinity also greatly decreased compared to the crystallinity of mPP.

Table 2. Long Period Calculated from $I(s)^2$ versus s^{-1} Plots of SAXS Data

sample	long period, equatorial scan (nm)
mPP	12.27
PH3.1	11.05
PH 9.7	10.05
PH13.9	12.00
PH22.4	16.10

For PH13.9 and PH22.4, the typical monoclinic iPP crystallographic form disappeared. Instead, three new peaks emerged in the X-ray diffraction pattern at $2\theta = 10.25$, 17.65, and 21.7°. The peak at $2\theta = 20.7°$ was broader than the other two peaks, which suggested that it was composed of two or more peaks. The amount of this new crystallographic form was larger in PH22.4 than in PH13.9. This fact implied that the new crystal form consisted, at least in part, of chain segments containing hexene units.

The most probable structure would be that of poly-(1-hexene) crystals. As described by Turner-Jones,[31] poly(1-hexene) crystallizes either in a higher-density orthorhombic form or a lower-density monoclinic form. Both forms are characterized by a strong X-ray reflection at a low angle of 4.05°, corresponding to the spacing of 1.09 nm. However, no such reflection was found in WAXS patterns of the PH copolymers under consideration. The WAXS pattern of PH22.4 shows only three reflections at $2\theta = 10.3$, 17.65, and 20.7° that correspond to those observed in the WAXS diffractogram (Figure 11). None of them agrees with the reported structures for poly(1-hexene).[31]

SAXS Results. The SAXS patterns obtained for mPP, PH3.1, PH 9.7, PH18.9, and PH22.4 compression molded films presented a diffuse ring. The long period was determined from the vertical and meridional scans, as taken from peaks in plots of $I(s)^2$ versus s, where I is the scattering intensity and $s = 2 \sin \theta/\lambda$ with $\lambda = 0.15418$ nm being the wavelength of the X-ray incident beam. The results are presented in Table 2.The long period of mPP was 12.2−12.3 nm. As the hexene content increased, the long period decreased to 11.0 nm for PH3.1 and to 10.0 nm for PH9.7. Simultaneously the scattering intensity decreased until only a faint ring was visible in the SAXS pattern of PH9.7. As the hexene content increased further, the long period re-emerged. The new SAXS ring with long period of 12.0 nm was rather strong in PH13.9 and stronger in PH22.4, with long period of 16.1 nm. The trends were consistent with the AFM observations, although the lamellar thickness from AFM was significantly higher than from SAXS, especially for mPP. Others who observed this discrepancy attributed it to a broad distribution of lamellar thicknesses and the resulting uncertainty in interpreting the diffuse SAXS maximum.[32]

Crystallographic Unit Cell of the New Phase. To identify the crystallographic unit cell and the X-ray reflections, deformed specimens of PH22.4 were prepared. The sample in the form of a $3.8 \times 11.7 \times 22$ mm^3 rod was deformed in a channel die to a compression ratio of 6.8 at ambient temperature at a rate of 0.5 mm min^{-1}. The true stress−compression ratio curve of PH22.4 is presented in Figure 12. After compression, the specimen was allowed to relax for 15 min at the final compression

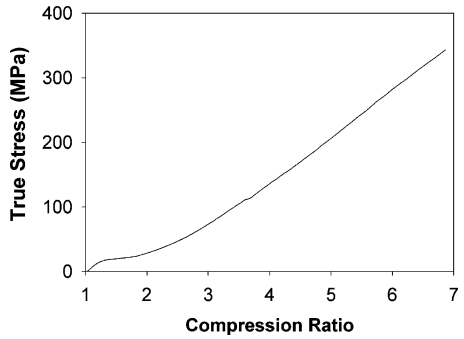

Figure 12. True stress versus compression ratio for PH22.4 compressed in a channel die at 22 °C at a rate of 0.5 mm min^{-1}.

ratio before the stress was released. The specimen recovered to a compression ratio of 3.4 and showed a fairly weak texture, as seen from rather broad reflections in the WAXS pattern. After 12 h at the final compression ratio of 6.8, the deformed specimen showed almost no anisotropy of crystal orientation, indicating that it had completely relaxed and recrystallized.

To obtain a stronger texture, 0.22 mm thick compression-molded films aged for 2 weeks at 22 °C were stretched in a tensile testing machine to various draw ratios. Drawing beyond the elastic region produced shear bands at 45° that gradually spread over the entire gauge length. As the draw ratio exceeded 2.5−3.0, the shear bands reoriented perpendicular to the draw direction and finally disappeared. A draw ratio higher than 5.5 could not be obtained without fracturing the specimen. The gauge section of the specimen was 21 mm in length and width. Such a geometry was chosen in order to obtain a large contribution of plane strain deformation which would make it possible to differentiate orientation in the plane perpendicular to the draw direction. After deformation to a local draw ratio of 5.5, determined from the displacement of ink marks, the width of the specimen was reduced to 11.5 mm whereas the thickness was reduced from 0.22 mm to 0.075 mm. By this means, the specimen changed less in the width than in the thickness, and thereby the texture was differentiated from a pure fiber texture. Part of the stretched film from the gauge section, still under stress, was mounted in a special X-ray sample holder. The draw ratio was fixed at 5.5, and shrinkage was prevented by the clamps. The diffraction pattern of this specimen, presented in Figure 13a, showed five distinct reflections. The 2θ positions of these reflections were measured from diffractograms obtained in the transmission mode, Figure 13b, and are listed in Table 3. The azimuthal scan at $2\theta = 20.73°$ allows determination of the exact azimuthal positions of the X-ray reflections. The four-point reflections are positioned at azimuthal angles of 42.045°, 137.955°, 222.045°, and 317.955°. The fiber spacing (c axis, macromolecular chain direction) determination for the deformed PH22.4 specimen was based on the Laue equation:

$$\cos(\epsilon) = n\lambda/c \tag{2}$$

where ϵ is the diffraction angle measured from the equator, λ is the wavelength of the X-ray beam, n is the number of the level of reflection in the fiber direction (equatorial being the zero-level), and c is the fiber spacing. The reflection at $2\theta = 20.73°$ and at azimuthal angle $\mu = 42.045°$ in the first diffraction layer was considered. The position of this layer was corrected for the flat film by the following formula:

$$\tan(2\theta_1) = \tan(2\theta)\sin(\mu)[\tan^2(2\theta)\cos^2(\mu) + 1]^{-1/2} \tag{3}$$

where $\theta_1 = \epsilon$ is the vertical position of the first reflection layer on the circular film. For the reflection at $2\theta = 20.73°$ and at $\mu = 42.045°$, $\theta_1 = 13.712°$, which corresponds to a fiber spacing $c = 0.6458$ nm.

Following the method of Hull and Davey,[33,34] crystallographic indices were assigned to each of the equatorial reflections. The method is based on fitting the set of spacings obtained for equatorial reflections to the set of spacings obtained for assumed symmetry of the crystallographic unit cell. The method relies on the formula correlating the equatorial spacing to crystallographic indices presented below for the orthorhombic unit cell:

$$d(hk0) = (h^2/a^2 + k^2/b^2)^{-1/2} \tag{4}$$

where $d(hk0)$ is one of equatorial spacings obtained from the WAXS fiber diffraction pattern, and h and k are crystallographic indices corresponding to the a and b crystallographic axes, respectively. Crystallographic indices for the orthorhombic unit cell were assigned using the Hull−Davey chart.[34] The results are listed in Table 3.

The Hull−Davey plot also provides the b/a ratio, which for our case, is equal to 1.76. From the reflection at $2\theta = 17.65°$, identified as the (130) reflection, the value of a can be calculated from eq 4. For $h = 1$, $k = 3$ and $b/a = 1.76$, the value of $a = 0.9930$ nm. The value of b can be obtained from eq 3 for the reflection at $2\theta = 10.30°$, which is either the (110) or (020) reflection. For the spacing $d = 0.8588$ nm, the (110) index gives $b = 1.7176$ nm and the (020) index gives $b = 1.7227$ nm, the values being very similar. For the reflection at $2\theta = 20.60°$ indexed as (220) or (040), the d spacing calculated from values of a and b determined above is 0.4298 nm for the index (220) or 0.4294 nm for the index (040), whereas the experimentally measured spacing is 0.4311 nm. The agreement is fairly good in both cases.

To verify the crystallographic axes and distinguish between the alternative crystallographic indices of the reflections, pole figures were prepared for each of the reflections observed in Figure 13. The pole figures are presented in Figure 14. The reflections at $2\theta = 20.60°$ and $2\theta = 20.73°$ are on the same pole figure (Figure 14c) because the integral intensity data collection requires a wide opening of the receiving slit of the diffractometer. The two arcs represent clustering in the orientation of normals to the crystallographic planes that reflect X-rays at $2\theta = 20.73°$, whereas the two central leaves identify the normals of the crystallographic planes reflecting at $2\theta = 20.60°$. From uneven distribution of normals along the arcs corresponding to the planes reflecting at $2\theta = 20.73°$, it can be judged that there is a large contribution of plane strain during deformation. It is obvious that the reflection at $2\theta = 20.73°$ is produced by either ($h0l$) or ($0k1$) crystallographic planes because the maximum clustering of normals is meridional. A calculation shows that it is the (031) plane. Also, the tilt of the arcs from the equator by 38.7−42.1° is only slightly less than the angle of 42.045° between the ab (equatorial) plane and the (031) plane.

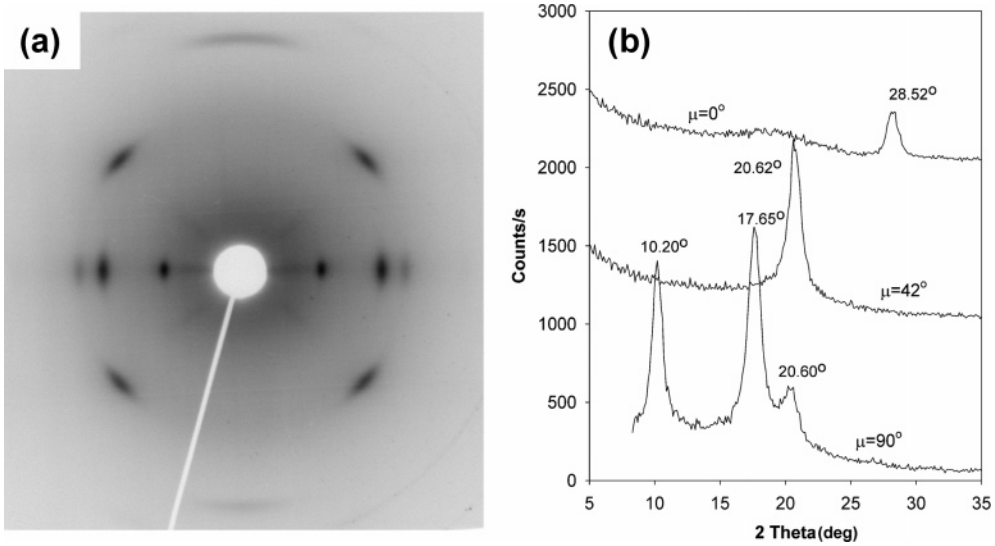

Figure 13. WAXS of PH22.4 film stretched to a draw ratio of 5.5 and held at fixed length: (a) WAXS pattern of the stretched film; and (b) 2θ scans at azimuthal angles of 0, 42, and 90° in the transmission mode.

Table 3. Positions of WAXS Reflections for Oriented PH22.4, Calculated Bragg Spacings, and Assigned Crystallographic Indices Assuming Orthorhombic Symmetry

diffraction angle (2θ) (deg)			d spacing[a]	peak	initial index from Hull–Davey chart	revised index from pole figure analysis
reflection	transmission	mean value	(nm)	position		
10.25	10.35	10.30	0.8588	equatorial	(110) or (020)	(210)
17.65	17.65	17.65	0.5025	equatorial	(130)	(230)
not seen	20.60	20.60	0.4311	equatorial	(220) or (040)	(040)
20.62	20.85	20.73	0.4285	42°		(031)
not seen	28.52	28.52	0.3129	meridional (broad)		(112)

[a] $d = \lambda/(2 \sin \theta)$, $\lambda = 0.15418$ nm.

The reflection at 20.60° arises from (0k0) planes. This is shown by clustering of normals at the equator at a small angle (+12.8° and −12.8°) from the center in the form of two nearly overlapped leaves. The splitting into two leaves results from incomplete plane strain deformation. The plane has the index (040). This observation suggests that the easiest crystallographic slip (most densely packed plane) during plastic deformation occurs along (0k0) planes.

The reflection at $2\theta = 28.52°$ lies at the second layer of the fiber diffraction, i.e., has the index $l = 2$. Clustering of normals in the pole figure (Figure 14d) for this plane forms a ring around the pole tilted at 10.5−11.5° away from the fiber axis. Complete indexing of this diffracting plane can be performed by trial and error fitting to the spacing of 0.3129 nm and to the tilt angle of the normal to this plane with respect to the c axis of 10−11°. It appears that the best fit of the spacing and the angle is achieved if the plane intersects the a axis at $2a$, the b axis at b, and the c axis at $c/2$. The resulting spacing is 0.3133 nm, and the tilt angle is 10.6°. It follows that the calculation of the a axis should be revised to twice the previous value giving $a = 1.9860$ nm. The revised index of the plane reflecting at 28.52° is (112), Table 3. Revised values of the indices of other diffracting planes are accordingly (210) to planes reflecting at 10.30° and (230) to planes reflecting at 17.65°. Assignments of (040) to planes reflecting at 20.60° and (031) to planes reflecting at 20.73° remain unchanged.

The correctness of the indexing can be tested by analysis of the other pole figures. Normals to the crystallographic planes diffracting at $2\theta = 10.30°$ cluster in two distinctly separated equatorial leaves (Figure 14a). The pole figure is significantly different from that of $2\theta = 20.60°$ reflections (Figure 14c), which was identified with the (040) plane. It is therefore the (110) plane. Calculation of the angle between the bc plane and the (110) plane gives 30.03°. It follows that the separation between the two leaves of clustering for perfect plane strain deformation with the easiest slip plane being the (0k0) should be of the order of 60°. In fact, separation of the concentration leaves as estimated from the pole figure is about 56−58°, again in good agreement with the prediction.

Stress–Strain Behavior. Homopolymer and PH copolymers with low hexene content deformed in a manner characteristic for semicrystalline thermoplastics with highly localized yielding, formation of a well-defined neck, and an extended region of cold drawing, Figure 15. With increasing hexene content, the modulus decreased, the yield stress decreased, the neck became more diffuse, and the natural draw ratio decreased. Although necking became progressively more diffuse as hexene content increased, nonuniform deformation with a distinct neck persisted in PH25.1. In contrast, a PO copolymer with slightly lower comonomer content, PO22.7, deformed uniformly at a lower stress level. The yield stress of PH copolymers containing less than 10 mol% comonomer decreased logarithmically with comonomer content in accordance with the relationship reported previously for PO copolymers.[8] However, due to the new crystal form of PH, copolymers containing more than 10 mol% hexene exhibited higher yield stress than PO copolymers of comparable comonomer content.

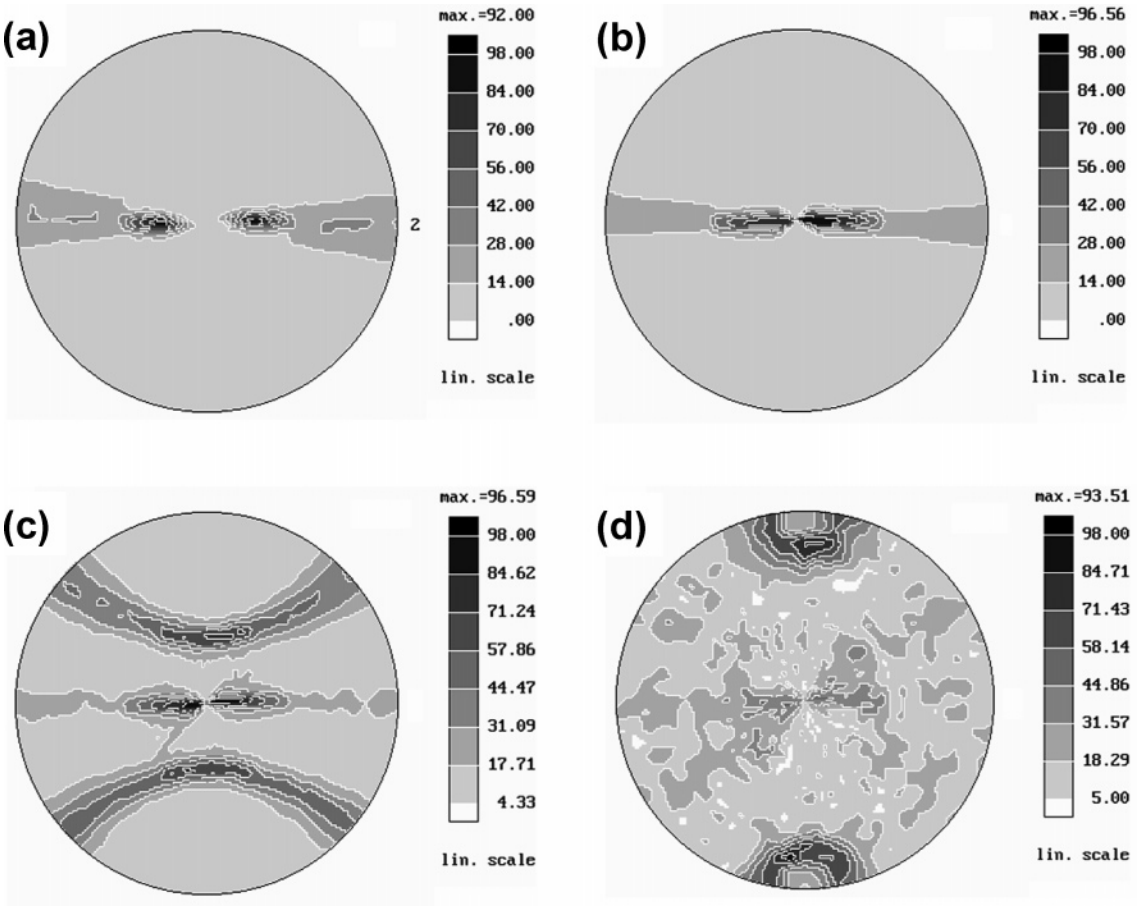

Figure 14. Pole figures of PH22.4: (a) normals to the planes reflecting at $2\theta = 10.30°$; (b) normals to the planes reflecting at $2\theta = 17.65°$; (c) normals to the planes reflecting at $2\theta = 20.60°$ and 20.73°; and (d) normals to the planes reflecting at $2\theta = 28.52°$. Equal area projection, stereographic projection, and gray level.

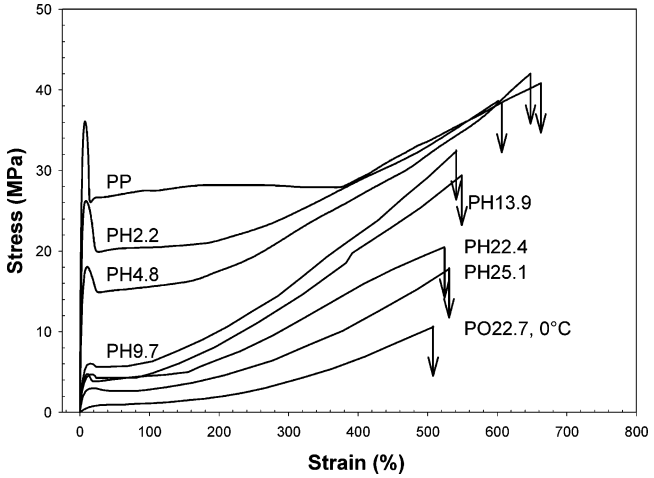

Figure 15. Tensile stress−strain curves of PH copolymers. Data for a PO copolymer with 22.7 mol% octene from ref 8.

Conclusions

The thermal, morphological, and mechanical properties of random PH copolymers are reported. The crystallinity of PH copolymers decreases smoothly with increasing hexene content up to about 10 mol%. Also, the melting and peak crystallization temperatures decrease with increasing hexene content. For PH copolymers with less than 10 mol% hexene, increasing comonomer content affects crystallization in the way that would be expected if comonomer were excluded from the polypropylene crystal. The PH copolymers that contain more than 10 mol% hexene crystallize with a new crystal structure that permits incorporation of hexene units. Nucleation of the new crystal form is slow, and once nucleated, the lamellae grow to become very long.

The copolymer with 3.1 mol% hexene has about 35 wt% crystallinity and, like mPP, crystallizes as α-positive spherulites. However, the spherulites are smaller and lamellae are thinner than in mPP. Unlike mPP, polypropylene with 3.1 mol% hexene crystallizes almost exclusively in the γ-form. At 4.8 and 9.6 mol% hexene, the spherulites become negative due to inhibition of crystallographic branching. Copolymers with 9.7 mol% hexene exhibit low crystallinity with the distorted α-form of polypropylene. All these materials exhibit thermoplastic behavior characterized by yielding with formation of a sharp neck, cold drawing, and strong strain hardening.

Copolymers with more than 10 mol% hexene have crystallinity in the range of 10−15% based on the polypropylene crystal. Hexene units are thought to be integral to the crystal structure. This conclusion follows from observations that the crystallinity is higher than would be expected if comonomer were excluded from the crystal and the crystals become better developed as the hexene content increases. Copolymers with more than 10 mol% hexene crystallize slowly. When cooled to ambient temperature from the melt, an incubation period is required before primary nucleation occurs. Long fibrous lamellae, 10−15 nm in thickness, form around the nucleus. The lamellae rapidly become more numerous as they form sheaf-like arrays that develop

into small spherulites. The corresponding enthalpy change as a function of time assumes an S-shape characteristic of the phase transition described by the Avrami process. These materials also exhibit thermoplastic behavior although with formation of a diffuse neck at a relatively low yield stress.

The long period as measured by SAXS systematically changes according to the crystallographic form. In mPP, well-developed stacks of lamellae have a periodicity of 12.2 nm, the long period decreases to 11.0 nm for γ-form crystals of PH with 3.1 mol% comonomer and to 10.0 nm with low scattering intensity for the distorted α-form crystals of PH with 9.7 mol% comonomer. For PH with 13.4 mol% comonomer, the new crystalline form has long period of 12.0 nm and low scattering intensity, the long period increases to 16.0 nm, and the SAXS becomes very distinct for PH with 22.4 mol% comonomer.

The new crystallographic form has not been reported for either polypropylene or for poly(1-hexene). It follows from WAXS studies of highly oriented films of the copolymer with 22.4 mol% hexene that the crystallographic unit cell has orthorhombic symmetry with $a = 1.9860$ nm, $b = 1.7176$ nm, and $c = 0.6458$ nm. The most intense diffracting planes are identified as the (210) plane reflecting at $2\theta = 10.30°$, the (230) plane reflecting at $2\theta = 17.65°$, the (040) plane reflecting at $2\theta = 20.60°$, the (031) plane reflecting at $2\theta = 20.73°$, and the (112) plane reflecting at $2\theta = 28.52°$ for Cu Kα radiation. Based on pole figures, it is evident that the easiest slip during plastic deformation of the new crystal form occurs along (0k0) planes.

Acknowledgment. The technical assistance of Dr. Matt Bishop, The Dow Chemical Company, for synthesis of the polymers and Dr. Angela Taha, The Dow Chemical Company, for NMR analysis is gratefully acknowledged. This research was generously supported by The Dow Chemical Company.

References and Notes

(1) Bensason, S.; Minick, J.; Moet, A.; Chum, S.; Hiltner, A.; Baer, E. *J. Polym Sci., Part B: Polym. Phys.* **1996**, *34*, 1301−1315.
(2) Chen, H.; Guest, M. J.; Chum, S.; Hiltner, A.; Baer, E. *J. Appl. Polym. Sci*. **1998**, *70*, 109−119.
(3) Galimberti, M.; Piemontesi, F.; Fusco, O. *Metallocenes as Catalysts for the Copolymerization of Ethene with Propene and Dienes. In Metallocene-based Polyolefins*; Scheirs, J., Kaminsky, W., Eds.; Wiley: New York, 2000; Vol 1, pp 309−343.
(4) Bicerano, J. *Rev. Macromol. Chem. Phys*. **1998**, *C38*, 391−479.
(5) Arnold, M.; Henschke, O.; Knorr, J. *Macromol. Chem. Phys*. **1996**, *197*, 563−573.
(6) Spaleck, W. *Synthesis and Properties of Metallocene Catalysts for Isotactic Polypropylene Production. In Metallocene-based Polyolefins*; Scheirs, J., Kaminsky, W., Eds.; Wiley: New York, 2000; Vol. 1, pp 401−424.
(7) Minick, J.; Moet, A.; Hiltner, A.; Baer, E.; Chum, S. P. *J. Appl. Polym. Sci*. **1995**, *58*, 1371−1384.
(8) Poon, B.; Rogunova, M.; Chum, S. P.; Hiltner, A.; Baer, E. *J. Polym. Sci., Polym. Phys*. **2004**, *42*, 4357−4370.
(9) Paukkeri, R.; Lehtinen, A. *Polymer* **1993**, *34*, 4075−4082.
(10) Galante, M. J.; Mandelkern, L.; Alamo, G. R.; Lehtinen, A.; Paukkeri, R. *J. Therm. Anal*. **1996**, *47*, 913−929.
(11) Gahleitner, M.; Bachner, C.; Ratajski, E.; Rohaczek, G.; Neibl, W. *J Appl. Polym. Sci.* **1999**, *73*, 2507−2515.
(12) Shin, Y.-W.; Hashiguchi, H.; Terano, M.; Nitta, K. *J. Appl. Polym. Sci*. **2004**, *92*, 2949−2954.
(13) Brandrup, J.; Immergut, E. H. *Polymer Handbook*, 3rd ed.; Wiley: New York, 1989; p V29.
(14) Hemsley, D. A. *The Light Microscopy of Synthetic Polymers*; Oxford University Press: Oxford, 1984.
(15) Galeski, A.; Bartczak, Z.; Argon, A. S.; Cohen, R. E. *Macromolecules* **1992**, *25*, 5705.
(16) Forlini, F.; Tritto, I.; Locatelli, P.; Sacchi, M. C.; Piemontesi, F. *Macromol. Chem. Phys.* **2000**, *201*, 401−408.
(17) Kissin, Y. V.; Brandolini, A. J. *Macromolecules* **1991**, *24*, 2632−2633.
(18) Babu, G. N.; Newmark, R. A.; Chien, J. C. W. *Macromolecules* **1994**, *27*, 3383−3388.
(19) Burfield, D. R. *Macromolecules* **1987**, *20*, 3020−3023.
(20) Burfield, D. R.; Loi, P. S.; Doi, Y.; Mejzík, J. *J. Appl. Polym. Sci*. **1990**, *41*, 1095−1114.
(21) Burfield, D. R.; Kashiwa, N. *Makromol. Chem*. **1985**, *186*, 2657−2662.
(22) Passaglia, E.; Martin, G. M. J Res NBS A. *Phys. Chem*. **1964**, *68A*, 519−527.
(23) Passaglia, E.; Kevorkian, H. K. *J. Appl. Phys*. **1963**, *34*, 90−97.
(24) Arnold, M.; Bornemann, S.; Köller, F.; Menki, T. J.; Kressler, *J. Macromol. Chem. Phys*. **1998**, *199*, 2647−2653.
(25) Padden, F. J.; Keith, H. D. *J. Appl. Phys*. **1973**, *44*, 1217−1223.
(26) Norton, D. R.; Keller, A. *Polymer* **1985**, *26*, 704−716.
(27) Natta, G.; Corradini, P. *Nuovo Cimento*, *Suppl*. **1960**, *15*, 40.
(28) Brueckner, S.; Meille, S. V. *Nature* **1989**, *340*, 455.
(29) Meille, S. V.; Brueckner, S.; Porzio, W. *Macromolecules* **1990**, *23*, 4114.
(30) Lotz, B.; Graff, S.; Straupe, C.; Wittmann, J. C. *Polymer* **1991**, *32*, 2902.
(31) Turner Jones, A. *Makromol. Chem*. **1964**, *71*, 1−32.
(32) Hosier, I. L.; Alamo, R. G.; Lin, J. S. *Polymer* **2004**, *45*, 3441−3455.
(33) Hull, A. W.; Davey, W. P. *Phys. Rev*. **1921**, *17*, 549.
(34) Alexander, L. E. *X-ray Diffraction Methods in Polymer Science*; Wiley: New York, 1968; pp 50−63.

MA048813L